Fourier transform infrared spectroscopy of electronic excitations to probe magnetic order and phase transitions in solid oxygen

S. A. Medvedev,[1,2] A. P. Brodyanski,[1] and H. J. Jodl[1,3]
[1]*Fachbereich Physik, Universität Kaiserslautern, Erwín Schrödinger Strasse, D 67663 Kaiserslautern, Germany*
[2]*Kharkov State Polytechnical University, 21, Frunze Street, 310002, Kharkov, Ukraine*
[3]*LENS, European Laboratory for Non Linear Spectroscopy, Largo E. Fermi 2, I-50125 Firenze, Italy*
(Received 15 November 2000; published 19 April 2001)

Systematic Fourier transform infrared (FTIR) spectroscopic investigations of interaction-induced electronic transitions $^3\Sigma_g^- - ^1\Delta_g$ ($v=0,\ldots,3$) of solid and liquid oxygen were carried out in the temperature range 10–90 K at ambient pressure. We interpret these absorption bands as phonon sidebands to an electronic (or an electronic-vibrational) excitations plus (in α-O_2) exciton (-vibron)-magnon bound states. A consistent description of electronic spectra in *all* phases of oxygen (α, β, γ, liquid) was achieved. It was shown that the combined excitations are assisted by a spin-spin exchange interaction in condensed phases of oxygen. A special procedure to analyze the band shape of these spectra was worked out to determine the unknown frequencies of electronic and electronic-vibrational excitations. The magnon frequencies at boundaries of the Brillouin zone were deduced from electronic-vibrational spectra and their temperature behaviors were explored in magnetically ordered α-O_2. We present several unambiguous direct experimental proofs that the α-β phase transition is of first order and we show that there are no experimental evidences for magnetic disordering as well as for temperature-caused changes in crystal structure in α-O_2 as a precursor to the α-β phase transition. We investigated the kinetics of the α-β phase transition and we found out an extreme sensitivity of this transition to impurities (as small as 1 ppm). We discovered that the frequencies of electronic and electronic-vibrational excitations depend strongly on magnetic order in the α phase and that they are hardly ruled by changes in molar volume in all phases. Thus, spectroscopy of electronic excitations can be used to probe indirectly the magnetic order and to classify the order of phase transitions in high-pressure phases of solid oxygen, where this information is not available up to now.

DOI: 10.1103/PhysRevB.63.184302 PACS number(s): 63.20.Ls, 78.30.−j, 75.50.Xx, 61.50.Ks

I. INTRODUCTION

Solid oxygen is a unique crystal. It combines properties of a cryocrystal and a magnet, transforms from transparent to color at increasing pressure and becomes a metallic molecular crystal and, further on, behaves like a superconductor at higher pressure. These unusual features originate from peculiarities of electronic structure of the O_2 molecule: such as a nonzero electronic spin in the ground electronic state $^3\Sigma_g^-$ and two low-lying electronic levels ($^1\Delta_g$ and $^1\Sigma_g^+$ at 7882.4 cm^{-1} and 13 121 cm^{-1}) above the ground state.[1] Therefore, the electronic spectra contain important information on magnetic characteristics of solid oxygen as well as on the physical origin of density (or pressure) -induced changes in the properties of this unique cryocrystal.

To our knowledge, there are only two publications concerning high-pressure optical spectra of solid oxygen[2] in which qualitative changes in spectra during β-ε and δ-ε phase transitions were studied. To clarify many unclear physical questions of oxygen at zero pressure and to form a basis for the following investigations at high pressure, systematic studies of electronic transitions at equilibrium vapor pressure are therefore necessary.

At ambient pressure, solid oxygen exists in three phases: γ-O_2 ($43.8 \leqslant T \leqslant 54.36$ K), β-O_2 ($23.87 \leqslant T \leqslant 43.8$ K) and α-O_2 at $T \leqslant 23.87$ K. The γ phase has a cubic crystal structure with eight molecules per unit cell (space group $Pm3n$): two molecules occupying the body-centered-cubic positions are orientationally disordered (''sphere-like'' molecules), whereas the other six molecules form linear chains running along three orthogonal $\langle 100 \rangle$ axes and their axes are almost stochastically distributed perpendicularly to these directions in crystal (''disklike'' molecules).[3,4] The orientationally ordered β (space group $R\bar{3}m$) and α (space group $C2/m$) phases possess a layered crystal structure: the distance between nearest neighboring molecules within the basal plane is substantially smaller than the one between molecules in adjacent layers.[3] The molecules in the basal planes are located at the tops of right hexagons in β-O_2 while a relatively small monoclinic distortion exists in α phase.[3] The high-temperature γ and β phases of solid oxygen possess no long-range magnetic order,[4,5] whereas the α phase is a two-sublattice antiferromagnet.[6]

The β-γ phase transition is accompanied by a big volume jump (about 5.4%) and its physical nature is quite well understood[7]—it is a pure structural phase transition driven by the competition between isotropic and anisotropic parts of the intermolecular interaction, accompanied by the changes in orientational order of the oxygen molecules. An exact classification of the α-β phase transition is missing up to now: this transition is characterized by very small changes in molar volume (less than 0.2%)[3] and available experimental data on latent heat measurements are contradictory.[8,9] The physical origin of this phase transition is unclear too: pure crystallographic transition,[10] magnetically driven,[11] and/or magnetoelastically driven.[12] Very recently, we applied a

matrix-isolation technique to probe the order of the α-β phase transition.[13] Monitoring the behavior of spectroscopic characteristics of CO molecules matrix isolated in solid oxygen, i.e. *indirectly*, we obtained strong experimental evidences that this transition is of first order.

Different experimental techniques such as Raman spectroscopy,[14,15] ir spectroscopy,[16] and inelastic neutron scattering[17] were applied to investigate elementary excitations in solid oxygen (magnon, libron, vibron) at the center of Brillouin zone. However, the behavior of these excitations is almost unexplored at Brillouin zone boundaries. Consequently, the energy spectra $\omega(\mathbf{k})$ of elementary excitations in solid oxygen are either completely unknown (vibron) or contradictory (magnons,[3,18,19] librons[3,19,20]). Only a qualitative picture exists for energy spectrum of excited electronic states in the α-oxygen.[21]

For the free oxygen molecule, transitions between the three lowest electronic states ($^3\Sigma_g^-$, $^1\Delta_g$, and $^1\Sigma_g^+$) are forbidden as electric dipole but allowed as magnetic dipole and electric quadrupole transitions[22] and characterized by very small absorption.[1] If density of oxygen gas is increased, broad ir-active bands, induced by the intermolecular interaction of a pair or a cluster of oxygen molecules, appear besides absorption of single O_2 molecules.[23,24] In compressed gases (density $\rho > 5$ Amagat) and in high-temperature phases of condensed oxygen, these interaction-induced bands become broader and their intensity grows by order of magnitude (in factor of 10^3-10^4).[23,25] A complicated fine structure appears in electronic spectra of the magnetically ordered low-temperature α phase.[21] Therefore, spectroscopic studies of electronic transitions can be used as a powerful tool to investigate peculiarities of intermolecular interaction, to probe magnetic order, and to clarify an order of solid-solid phase transitions.

Although electronic spectra of solid and liquid oxygen have been investigated for more than 40 years, no complete systematic spectroscopic studies were carried out up to now. Nothing is known, for example, about the frequencies of the $^3\Sigma_g^-$-$^1\Delta_g$ transitions even for compressed oxygen gas;[26] there is no consensus about the concrete physical nature of the absorption bands in electronic spectra of condensed oxygen.[27–29]

In this paper, we will present the results of systematic Fourier transform infrared (FTIR) spectroscopic studies of several electronic-vibrational transitions [$^3\Sigma_g^-$-$^1\Delta_g(0\text{-}v)$, $v=0,\ldots,3$] in condensed phases of oxygen at low temperature (10–90 K) and at low pressure ($P \leqslant 1.5$ bar). Due to excellent optical sample quality and modern FTIR technique, we were able to investigate all peculiarities in these spectra in details.

This paper is structured as follows. In the next chapter, we will describe our experimental procedure. Experimental results and discussion will be presented in Sec. III. First, we will propose an interpretation of the nature of ir-active electronic absorption bands and will describe our procedure to model the band shape of electronic spectra as well as to determine the frequencies of electronic and electronic-vibrational excitations. Second, we will analyze their temperature behavior and will show that these quantities can be used to probe magnetic order in oxygen crystal. Third, we will discuss physical mechanism of combined excitations in condensed oxygen basing on our spectroscopic results. Fourth, we will determine the magnon frequencies at Brillouin-zone boundaries and will explore their temperature behavior in the α phase. Fifth, we will clarify the order and the physical nature of the α-β phase transition. Sixth, we will quantitatively analyze the kinetics of the α-β phase transition and will demonstrate an extreme sensitivity of this transition to small concentrations of impurities (ppm).

II. EXPERIMENTAL PROCEDURE

We investigated liquid and solid oxygen by FTIR spectroscopy in the temperature range from 10 to 90 K both at equilibrium vapor pressure and below 1.5 bars. The spectra of electronic transitions of oxygen [$^3\Sigma_g^-$-$^1\Delta_g(0\text{-}v)$, $v=0,1,2,3$, and $^3\Sigma_g^-$-$^1\Sigma_g^+(0\text{-}0)$ and (0-1)] were recorded in the near-ir and visible (red) spectral region (from 7000 to 15 000 cm^{-1}) by a Fourier spectrometer (Bruker IFS 120 HR). A tungsten lamp and two sets of beam splitters with suitable detectors were used: Si on CaF_2 as beam splitter and liquid-N_2-cooled InSb detector (accessible spectral range 1900–10 000 cm^{-1}) as well as dielectric coating on quartz as beam splitter and Si diode as detector (accessible spectral range 8000–20 000 cm^{-1}). The diameter of diaphragm was 0.8–1.0 mm and 1.0–1.5 mm, respectively. The frequency resolution was varied from 0.1 to 3 cm^{-1} depending on bandwidth of interest in spectra. The spectra of oxygen sideband to fundamental vibrations (mid-ir spectral region) were also recorded for comparison with the ones of electronic transitions. A glowbar source, KBr beam splitter and liquid-N_2-cooled MCT detector were used in this case (accessible spectral range 800–5000 cm^{-1}). The diameter of diaphragm and the frequency resolution were 1 mm and 0.5 cm^{-1}, respectively.

We used in our experiments an oxygen gas of 99.998% purity. Two series of samples were investigated: pure oxygen and oxygen enriched by 0.9 ppm of CO. The concentration of CO in solid oxygen was determined by using known absorption coefficient[30,13] by measuring the integrated intensity of the fundamental band of CO molecules matrix isolated in our samples. A specially designed sample cell with diamond windows (aperture 3 mm) was attached to the cold finger of He-closed-cycle cryostat to achieve low temperatures. The temperature was measured by a calibrated Si diode directly attached to the sample cell. Temperature resolution was 0.005 K at $T \leqslant 25$ K and 0.04 K at higher temperatures. Our crystal samples ($\varnothing 10 \times 1.2$ mm^2) were obtained in the following manner. The purged and evacuated cell was cooled down to 87 K and the investigated gas was liquefied at a pressure of 1.2–1.5 bar. To ensure good thermal contact of our sample with walls of the sample chamber, especially during crystal growth and solid-solid phase transitions, this gas pressure was maintained during the whole experiment. The crystals of γ-oxygen were slowly grown from liquid to obtain samples with good optical quality. To conquer the difficulties connected with the big volume jump at the $\gamma \rightarrow \beta$

phase transition we grew a crystal of β-O_2 mainly following the procedure worked out in Ref. 31 to grow single crystals of solid oxygen (for details see Ref. 13).

The grown crystals were completely transparent to visible light in all phases of solid oxygen controlled by eye (microscope). To characterize the quality of our crystal quantitatively we measured the spectra of the electronic $^3\Sigma_g^-$-$^1\Sigma_g^+(0\text{-}0)$ transition that exists in α-oxygen as a single peak and that disappears at the α-β phase transition. The full width at half maximum (FWHM) of this band (band maximum frequency of 13 167.08 cm^{-1}) was 1.1 cm^{-1} at 11 K in our samples in comparison to about 3 cm^{-1} at 1.5 K in samples grown by Prikhotko *et al.*[32] We could not detect any traces of ir-inactive O_2 vibron in our mid-ir spectra. Consequently, our crystals of low-temperature phases of solid oxygen are perfect.

III. RESULTS AND DISCUSSION

A. Description of spectra

In this investigated spectral region, we observed four absorption bands that belong to the $^3\Sigma_g^-$-$^1\Delta_g$ transition: one pure electronic (0-0) and three vibronic ones (0-1, 0-2, and 0-3). In spite of an enormous number of publications concerning different electronic spectra in oxygen, there is almost no concrete experimental information about this transition ($^3\Sigma_g^-$-$^1\Delta_g$) available. Spectra $^3\Sigma_g^-$-$^1\Delta_g$ (0-0 and 0-1) of liquid O_2 ($T>70$ K) and γ-O_2 ($T=86$ K) at pressure up to 8000 bars were investigated mainly to obtain data on integrated intensity of these bands as function of density.[23] These spectra were also recorded in liquid oxygen at $T=77$ K.[33] Concerning β oxygen we only found an illustrative picture of a $^3\Sigma_g^-$-$^1\Delta_g(0\text{-}0)$ spectrum at 30 K.[34] In α oxygen, spectra of these transitions were only measured at two temperature points: 21 K [Ref. 25] and 1.5 K.[2]

The absolute values of integrated intensity of the $^3\Sigma_g^-$-$^1\Delta_g$ bands are 149.24, 83.20, 5.55, and 0.42 cm^{-1} at 11.2 K in our samples for vibrational quantum number $v=0$, 1, 2, and 3, respectively. The normalized values obtained by us (1: 0.56: 0.04: 0.003) coincide quite well with data obtained by others at 1.5 K (1: 0.69: 0.06) [Ref. 21] and at 21 K (1: 0.33: 0.05: 0.009).[25] The positions of main maxima of each band agree very well with available data.[21,25] The fine structure, observed already at 1.5 K,[21] was also clearly observable in our spectra ($v=0,1,2$) up to 17 K due to high optical quality of our samples.

The temperature evolution of two absorption bands $^3\Sigma_g^-$-$^1\Delta_g$ (0-0 and 0-1) is shown in Fig. 1. The following general features are clearly visible.

(i) The pure electronic and vibronic transitions appear in *all* condensed phases of oxygen as broad absorption bands extending for some hundred wave numbers. A general decrease in absorbance is observed with increasing temperature. Two solid-solid phase transitions alter the spectra in different manner. At the $\alpha\rightarrow\beta$ phase transition ($T\sim24$ K), the bandwidth remains almost the same, whereas the absorbance decreases (by a factor of about 1.5 less in β phase). At the $\beta\rightarrow\gamma$ phase transition ($T\sim44$ K), the bandwidth drastically decreases and so does the absorbance.

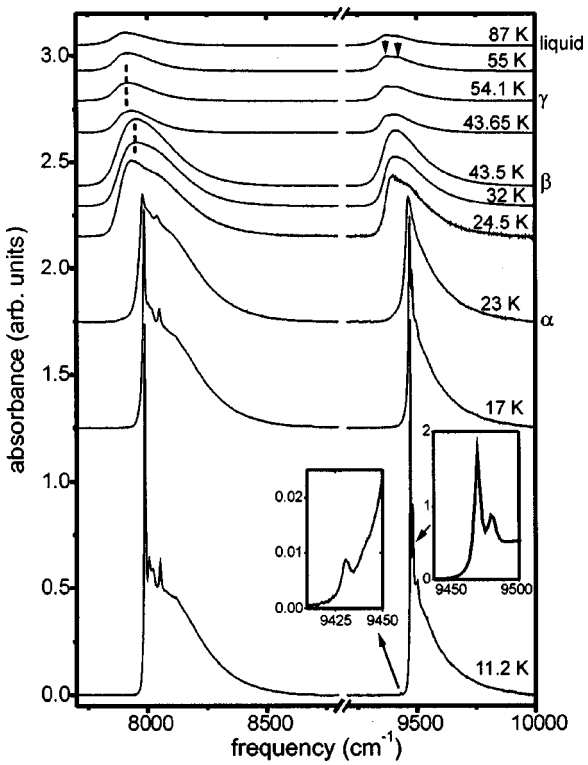

FIG. 1. Temperature evolution of $^3\Sigma_g^-(0)$-$^1\Delta_g(v)$ electronic absorption bands ($v=0,1$).

(ii) Both absorption bands are displaced as a whole toward lower frequency at the $\alpha\rightarrow\beta$ phase transition by a big jump, whereas at the $\beta\rightarrow\gamma$ phase transition by a small jump. Very small changes in spectra are observed during melting.

(iii) Spectra of both bands possess additional fine structure in the α-O_2. The first two sharp peaks are more pronounced in the spectrum of the 0-1 band (see the right inset in Fig. 1), whereas other peculiarities are more prominent in the 0-0 band spectrum. As temperature increases, this fine structure in both spectra is shifted toward lower frequencies, becomes broader and less pronounced. However, they remain observable up to the α-β phase transition point, particularly in the 0-0 band.

(iv) Two peculiarities are clearly observable in 0-1 absorption spectra of the γ- and liquid oxygen (shown by arrows in Fig. 1 right up). The qualitatively similar $^3\Sigma_g^-$-$^1\Delta_g(0\text{-}1)$ spectra were already observed in compressed oxygen gas[24] and interpreted as a superposition of two bands, i.e., the low-frequency component arises from an excitation of a molecule into first exciter vibrational level of $^1\Delta_g$ state: $^3\Sigma_g^-(0)+{}^3\Sigma_g^-(0)\rightarrow{}^1\Delta_g(1)+{}^3\Sigma_g^-(0)$ transition. The second band results from a simultaneous excitation of both molecules into high energetic states—one molecule is excited into ground vibrational level of $^1\Delta_g$ state, while the second molecule undergoes a transition to the first excited vibrational level of ground electronic state: $^3\Sigma_g^-(0)+{}^3\Sigma_g^-(0)\rightarrow{}^1\Delta_g(0)+{}^3\Sigma_g^-(1)$ transition.

The temperature behavior of 0-2 and 0-3 absorption bands is, in general, qualitatively similar to the behavior of the 0-1 band.

B. Nature of these electronic transitions and modeling their spectra

1. General approach

The most prominent spectral feature of the transitions $^3\Sigma_g^-$-$^1\Delta_g$ is a broad absorption band (several hundred cm^{-1}) that persists in *all* phases of condensed oxygen (Fig. 1). A similar band profile due to collision-induced processes is also observed in spectra of compressed oxygen gas.[24,35] We found in literature several assumptions to explain the nature of this broad absorption band. The fact that this feature exists in all phases indicates that this characteristic in spectra cannot be associated with an exciton-magnon sideband proposed in Ref. 27. Furthermore, the absorption band was assigned to be a usual exciton band in solids (or a superposition of two such bands) according to Ref. 28; however, typical bandwidth of pure exciton bands is a few cm^{-1} only. If we compare the spectrum of an electronic transition $^3\Sigma_g^-$-$^1\Delta_g$ to a spectrum in the fundamental region, we can recognize their principal similarity. Both kinds of spectra possess a specific substantially asymmetric band profile—a steep low-frequency edge and a widely extending high-frequency wing; as temperature decreases, this asymmetry becomes more pronounced in both cases. The fine structure appearing in electronic spectra in the α phase besides the broad band is similar to the additional maxima in spectra of the vibron sideband in orientationally ordered phases [compare, e.g., Fig. 1 to the spectrum of the vibron sidebands in α-N_2 and in α-O_2 shown in Figs. 2(a) and 2(b)]. Since such a broad band in the fundamental region is usually assigned to be a phonon sideband to internal vibrations (see, e.g., Ref. 36), we may interpret this broad band in the electronic region as a phonon sideband to an electronic or to an electronic-vibrational excitations. A similar interpretation of the 0-0 electronic band as the libron-assisted absorption band was already proposed by Fujiwara,[29] who tried to calculate the exciton frequency in the α-O_2 theoretically. Our idea is to determine the band origin frequencies (as ZPL) from the analysis of the experimental band profile directly, i.e., by dividing a phonon sideband profile into ''Stokes'' and ''anti-Stokes'' components. We successfully tested this approach by analyzing ir-active phonon sidebands to internal vibrations (solid nitrogen and condensed oxygen) and showed that the ZPL frequency (ω_0) determined by this procedure corresponds to the frequency of the internal oscillations of the *single* molecule in crystal.[37] For sake of clarity, the brief description and some illustrations of this approach will be present below.

In general, an ir-active combination band is formed by two different kinds of combined processes—additive and substractive combinations of a highly energetic excitation (e.g., electronic or vibrational excitation) with lattice excitations (phonons). Then additive combinations $\hbar\omega_1=\hbar\omega_0+\hbar\omega_{\rm ph}$ will produce a high-frequency wing ($\omega_1\geqslant\omega_0$), whereas subtractive combinations $\hbar\omega_2=\hbar\omega_0-\hbar\omega_{\rm ph}$ will form a low-frequency edge in the spectrum at $\omega_2\leqslant\omega_0$ ($\omega_{\rm ph}$ is a frequency of phonon involved).

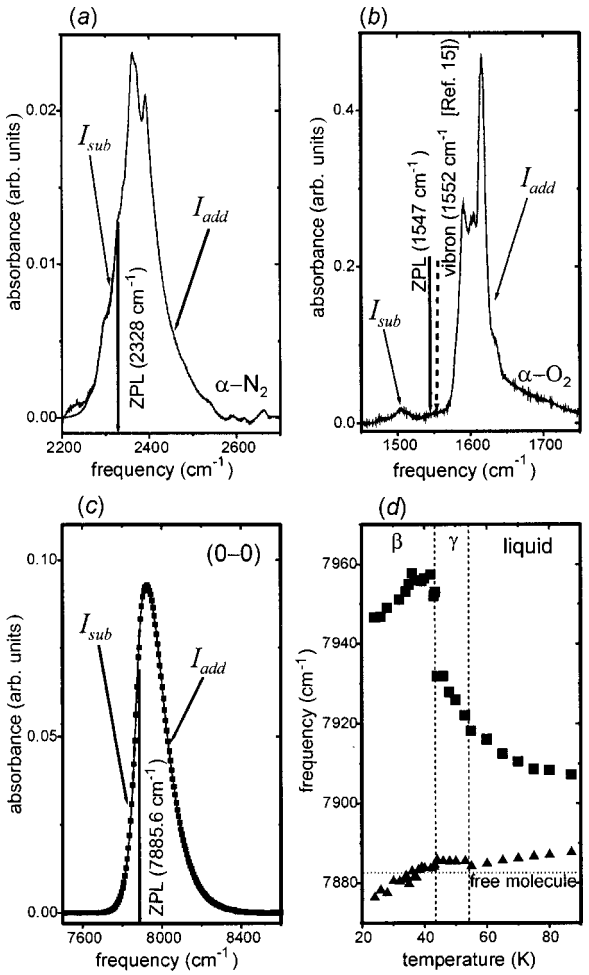

FIG. 2. Determination of band origin frequency by dividing the band spectra into ''Stokes'' ($I_{\rm add}$) and ''anti-Stokes'' ($I_{\rm sub}$) components: sidebands to internal vibrations in the α-N_2, $T=34.8$ K (a) and in the α-O_2, $T=23.3$ K (b); the phonon sideband to the $^3\Sigma_g^-$-$^1\Delta_g$(0-0) electronic excitations (γ-O_2, $T=50$ K) (c). (d) shows a comparison between the frequency of $^3\Sigma_g^-$-$^1\Delta_g$(0-0) band maximum (quadrate) and frequency of electronic excitations (triangle), obtained by our procedure.

It is well known (see, e.g., Ref. 38) that an infrared absorption intensity of additive ($I_{\rm add}$) and substractive ($I_{\rm sub}$) combined processes is described as follows:

$$I_{\rm add}(\omega_1=\omega_0+\omega_{\rm ph})\sim 1+n_{\rm exc}(\omega_0)+n_{\rm lat}(\omega_{\rm ph}=\omega_1-\omega_0), \tag{1a}$$

$$I_{\rm sub}(\omega_2=\omega_0-\omega_{\rm ph})\sim n_{\rm lat}(\omega_{\rm ph}=\omega_0-\omega_2)-n_{\rm exc}(\omega_0). \tag{1b}$$

Here $n_{\rm exc}(\omega_0)$ and $n_{\rm lat}(\omega_{\rm ph})$ are thermodynamic equilibrium occupation numbers of states with an energy $\hbar\omega_0$ and $\hbar\omega_{\rm ph}$, respectively, i.e., $n(\omega)=(e^{\hbar\omega/kT}-1)^{-1}$. Since $\hbar\omega_0/kT\gg 1$ at our experimental temperatures, $n_{\rm exc}(\omega_0)\approx 0$ and we can link both equations:

$$I_{\rm sub}(\omega_2=\omega_0-\omega_{\rm ph})=I_{\rm add}(\omega_1=\omega_0+\omega_{\rm ph})\exp(-\hbar\omega_{\rm ph}/kT) \tag{2}$$

Equation (2) is obviously similar to the well-known expression for Stokes and anti-Stokes intensities in Raman spectra.[38] The existence of Boltzmann factor in Eq. (2) causes the asymmetry in band profile of electronic absorption bands at every finite temperature. As temperature decreases occupation of phonon states decreases too. Consequently, an absorption caused by substractive combinations approaches zero as $T \rightarrow 0$. This is an explanation for the very sharp low-frequency edge of exciton sideband at low temperatures (see bottom of Fig. 1) like in Raman scattering at low temperatures, where there is no anti-Stokes component detectable.

Using Eq. (2), we can determine the ZPL frequency from the experimental sideband profile. Figures 2(a) and 2(b) illustrate our approach to analyze the vibrational sideband in the α-N_2 and the α-O_2. According to Ref. 39, the frequency of the internal vibrations of the single nitrogen molecules in the α-N_2 is equal to the degeneracy-weighted mean of two vibron frequencies (T_g and A_g modes) measured by Raman spectroscopy, i.e., 2327.8 ± 0.1 cm^{-1} at 34.8 K.[40] In case of the α-O_2, an estimate of the similar value can be obtained from the Raman spectroscopy measurements[41] for the $^{16}O_2$ fundamental in the sample with 20% $^{16}O_2$ in 80% $^{16}O^{18}O$ and $^{18}O_2 1548 \pm 1$ cm^{-1} at 15 K. The values 2328 ± 0.5 cm^{-1} (α-N_2, $T = 34.8$ K) and 1547 ± 0.5 cm^{-1} (α-O_2,23.3 K) obtained by us coincide quite well with the Raman data presented above. These results may be considered as the direct successful test of our approach. At the following analysis of the electronic absorption bands, we will presume that the ZPL frequencies of the electronic and electronic-vibrational phonon sidebands correspond to the frequencies of pure electronic and electronic-vibrational transitions similarly to the ones in case of the phonon sidebands to internal vibrations.

2. Application to high-temperature phases

Figure 2(c) illustrates the application of our procedure to determine the frequency of electronic excitations. Using this approach, we analyzed the electronic absorption bands in β-, γ-, and liquid oxygen and determined the frequency of $^3\Sigma_g^-(0)$-$^1\Delta_g(0)$ excitations as function of temperature [up triangle in Fig. 2(d)]. The statistical error of values obtained was less than 0.5 cm^{-1}. Frequencies of the band maximum of raw spectra (Fig. 1, broken lines left up) are also shown in Fig. 2(d) (quadrate) for comparison. Whereas the frequency of electronic excitations deviates relatively weakly from the one in the free molecule, the band maximum is characterized by considerably higher values. This difference between the position of band maximum and the frequency of the pure electronic transition corresponds to the frequency of the maximum of the phonon density of states (DOS) slightly modified by an unknown but mode-specific interaction between electronic and lattice excitations, according to our interpretation. The clear jump in frequency of band maximum at β-γ phase transition reflects qualitative changes in the phonon DOS at this structural phase transition.

Remarkably, first attempts to model an experimental profile of $^3\Sigma_g^-$-$^1\Delta_g$ absorption bands by dividing spectra into a high-frequency part and a low-frequency part modified by a Boltzmann factor were made at the end of 1960s years for spectra of compressed oxygen gas.[25,35] Because the band maximum was chosen as the band origin, no success was reached.

Now we can take the next step, i.e., to evaluate the band profile in spectra of vibronic transitions [$^3\Sigma_g^-$-$^1\Delta_g(0$-$v)$] in high-temperature phases of condensed oxygen (see Fig. 1, right up). Because the absorption band of these transitions actually consists of several single bands (e.g., two in 0-1 transition), we had to select some function to describe the shape of an individual band. We tested several analytical functions and their combinations and chose the asymmetric double sigmoidal[42] as the most suitable function to describe the ''Stokes'' part of the profile of absorption bands of $^3\Sigma_g^-$-$^1\Delta_g(0$-$0)$ electronic transitions [i.e., the analytical form of $I_{\mathrm{add}}(\omega)$ in Eq. (2)]. Then the absorption due to difference tones [$I_{\mathrm{sub}}(\omega)$] was reconstructed by using Eq. (2). A value of a ZPL frequency ω_0 and adjustable parameters of the asymmetric double sigmoidal (5 parameters) were considered as varying parameters, which must be determined to model the experimental spectrum. This analytic function provides together with Eq. (2) an excellent modeling of the band profile of $^3\Sigma_g^-$-$^1\Delta_g(0$-$0)$ absorption band at every temperature point in β-, γ-, and liquid oxygen. Figure 2(c) illustrates this result for γ-O_2. Since the deviation between experimental and modeled profiles is too small to be recognized in black and white picture, we had to use quadratic dots to mark the modeled profile. The band-origin frequencies found by this mathematical fit procedure coincide, within error less than 0.5 cm^{-1}, with values determined earlier by directly solving Eq. (2).

To describe a profile of the individual band belonging to the $^3\Sigma_g^-$-$^1\Delta_g(0$-$1)$ absorption band, we used the same approach. Two such single bands were superimposed to model the total profile of the 0-1 electronic-vibrational absorption band [Fig. 3(a), liquid O_2 at 75 K]. The agreement is excellent between the modeled (solid dots) and experimental (solid line) profiles. The sideband to the $^3\Sigma_g^-(0)$-$^1\Delta_g(1)$ electronic-vibrational excitations (band-origin frequency 9360.7 ± 0.5 cm^{-1}) and the sideband to the simultaneous combined excitation of $^3\Sigma_g^-(0)$-$^1\Delta_g(0)$ exciton plus $^3\Sigma_g^-(0$-$1)$ vibron (band-origin frequency 9420.5 ± 1.5 cm^{-1}) are shown by dashed and dash-dot lines, respectively.

3. Modeling spectra of α-oxygen

To analyze spectra of electronic transitions in α-O_2 a complete assignment of the fine structure in spectrum must be done. Six and four additional features are visible in these spectra of $^3\Sigma_g^-$-$^1\Delta_g(0$-$0)$ and $^3\Sigma_g^-$-$^1\Delta_g(0$-$1)$ transitions, respectively, at lowest temperature (Fig. 1). Analyzing the temperature evolution of the different peaks in the fine structure, the first two peaks possess a substantially stronger temperature dependence than the other ones. Consequently, we divided these features of fine structure into two different groups.

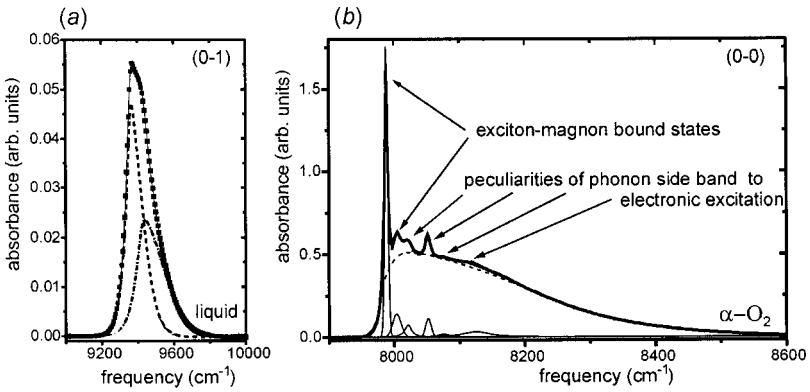

FIG. 3. Modeling spectra of electronic absorption bands by analytic functions (solid lines mark the experimental profiles). Interrupted lines in figure (a) show profiles of the individual bands modeled by asymmetric double sigmoid function; dots mark the total modeled profile. Dash line in figure (b) marks the asymmetric double sigmoidal describing the main part of profile of $^3\Sigma_g^-(0)$-$^1\Delta_g(0)$ electronic sideband.

Two first peaks of fine structure are situated at 7988.3 and 8003.7 cm^{-1} in spectrum of 0-0 band and at 9471.1 and 9480.8 cm^{-1} in 0-1 spectrum at 11.2 K. They were assigned[21] to a simultaneous creation of a $^3\Sigma_g^-$-$^1\Delta_g$ exciton (or a exciton-vibron in case of 0-1 absorption band) and a magnon at Brillouin-zone boundaries by one photon whose frequency equals a sum of exciton and magnon frequencies: $\omega_{\text{exc-mag}}^{\text{add}}=\omega_{\text{exc}}+\omega_{\text{mag}}$. The sharp profile of these doublets are caused by singularities of the magnon density of states at two points in **k** space: $\mathbf{k}_1\perp\mathbf{a}$, $k_1\approx\pi/b$ and $\mathbf{k}_2\perp\mathbf{b}$, $k_2\approx\pi/a$ (**a** and **b** are vectors of the unit cell in the basal plane of α-O_2). Further investigations on single crystals by polarized light[34] showed that the low- and high-frequency peaks of these doublets are completely polarized perpendicularly and along monoclinic axis **b** of α-O_2 unit cell, respectively.

Since the physical mechanism proposed in Ref. 21 corresponds to a usual absorption due to combined excitation of an exciton plus a magnon, similar sharp absorption peaks caused by simultaneous creation of an exciton and annihilation of a magnon would have to appear at $T\neq 0$ at the frequency of the difference tone: $\omega_{\text{exc-mag}}^{\text{sub}}=\omega_{\text{exc}}-\omega_{\text{mag}}$. The intensities of these ''Stokes'' and ''anti-Stokes'' components can be described by Eq. (2) too. Due to excellent optical quality of our samples and the modern spectroscopic technique used, the level of noise in our near-infrared (nir) spectra was less than 0.001 in comparison to the value of about 1.8 corresponding to an absorbance at the maximum of the most intensive exciton-magnon peak observed (see Fig. 1). Therefore, in spite of the existence of a damping Boltzmann factor, an anti-Stokes peak due to subtractive combination of an exciton and a magnon should be visible in our nir spectra; similar to an anti-Stokes component of the vibron sideband, which we clearly observed in our mid-ir spectra at $T\geqslant 17$ K. However, no traces of any additional peculiarities in the anti-Stokes part of the spectrum of $^3\Sigma_g^-$-$^1\Delta_g(0\text{-}0)$ absorption band were observed up to the α-β phase transition temperature. Consequently, only exciton-magnon combinations corresponding to a simultaneous creation of an exciton (or exciton-vibron) and a magnon are present in $^3\Sigma_g^-$-$^1\Delta_g$ absorption spectra according to experimental results.

The theoretical results[21] were obtained assuming the absence of a specific exciton-magnon interaction. Unfortunately, up to now a power of this interaction is not exactly known. However, there are some evidences that this interaction is not negligible and must be taken into account to describe correctly the optical spectra of α oxygen.[43] Then, presuming that the power of an exciton-magnon interaction is enough to form an exciton-magnon bound state we can explain why only the additive combinations of these electronic excitations—absorbing a photon—appear in spectra of electronic and electronic-vibrational transitions in magnetic ordered phase of solid oxygen.

Next two features are situated at about 8020.(6) and 8052 cm^{-1} in spectrum of 0-0 band and at about 9500.(6) and 9538.(6) cm^{-1} in 0-1 spectrum ($T=11.2$ K). They were interpreted[21] as libronic replicas of initial exciton-magnon doublet, i.e., as exciton (or exciton-vibron), magnon-libron combined excitations. Consequently, the ratio of intensities of these two peaks must qualitatively reproduce the one for the exciton-magnon doublet, which we discussed just before. Therefore, the feature at 8052 cm^{-1} should be substantially less intensive in comparison to the one at 8020.(6) cm^{-1}. Figure 1 (left) clearly shows that it is not the case. Moreover, the intensity of these two small features should also depend on the direction of polarized light in spectra of single crystal. However, no significant changes in intensity of these two peaks were observed.[34] Therefore, the assignment proposed in Ref. 21 is not consistent. We, instead, will assign these and all other small peaks in the fine structure to peculiarities of sideband to electronic excitations reflecting maxima of phonon DOS. Thus, we think that an electronic absorption band of α-O_2 is a superposition of the spectra caused by of exciton-magnon bound states and a phonon sideband to electronic excitations [Fig. 3(b)].

We modeled the profile of phonon sideband to the 0-0 electronic transition by the sum of an asymmetric double sigmoidal and Lorentzian functions describing the features of fine structure belonging to phonon sideband, whereas the exciton-magnon peaks were modeled by Gaussian functions. The divergence between total modeled and experimental profiles [Fig. 3(b)] is not observable at Fig. 3(b) scale used.

The spectrum of 0-1 absorption band was successfully modeled by superimposing the spectra due to two exciton-magnon bound states as well as due to phonon sidebands to the $^3\Sigma_g^-(0)$-$^1\Delta_g(1)$ electronic-vibrational excitation and to a simultaneous, combined excitation of $^3\Sigma_g^-(0)$-$^1\Delta_g(0)$ exciton plus $^3\Sigma_g^-(0\text{-}1)$ vibron. We assigned the fine structure features being additional to the exciton-magnon doublet to

TABLE I. Band origin frequencies determined by our modeling procedure ($T=11.2$ K).

Band	Frequency of band origin (cm^{-1})
$^3\Sigma_g^-(0)$-$^1\Delta_g(0)$	7982.9±1.5
$^3\Sigma_g^-(0)$-$^1\Delta_g(1)$	9467.1±3.8
$[^3\Sigma_g^-(0)$-$^1\Delta_g(0)+^3\Sigma_g^-(0$-$1)]$	9519.4±8.6
$^3\Sigma_g^-(0)$-$^1\Delta_g(2)$	10 924.2±1.6
$[^3\Sigma_g^-(0)$-$^1\Delta_g(1)+^3\Sigma_g^-(0$-$1)]$	11 004.8±6.6

peculiarities of $^3\Sigma_g^-(0)$-$^1\Delta_g(1)$ electronic-vibrational sideband. The similar approach was used to model the 0-2 absorption band, where three single bands related to three kinds of processes, $^3\Sigma_g^-(0)+^3\Sigma_g^-(0)\rightarrow{}^3\Sigma_g^-(0)+^1\Delta_g(2)$, $^3\Sigma_g^-(0)+^3\Sigma_g^-(0)\rightarrow{}^3\Sigma_g^-(1)+^1\Delta_g(1)$, and $^3\Sigma_g^-(0)+^3\Sigma_g^-(0)\rightarrow{}^3\Sigma_g^-(2)+^1\Delta_g(0)$ are involved. The agreement between modeled and experimental profiles was excellent.

The values of band-origin frequencies are presented in Table I for all kinds of electronic sidebands modeled by us ($T=11.2$ K). Because of very small total intensity of the third sideband involved in 0-2 absorption band, it was not possible to determine its parameters with high accuracy.

The left inset in Fig. 1 shows a small peak around 9430 cm^{-1} in spectra of 0-1 absorption band at $T\leqslant 15$ K. We interpret this peak as exciton-magnon-vibrational excitations of an oxygen isotope. Indeed, the frequency of this excitation of an $^{16}O^{18}O$ isotope isolated in $^{16}O_2$ crystal maybe estimated as the sum of the exciton-magnon frequency for $^{16}O_2$ molecules (7988.3 cm^{-1}) and the frequency of vibrational excitation of the isotope $^{16}O^{18}O$ in the $^1\Delta_g$ state. Using the known masses of the $^{16}O_2$ and $^{16}O^{18}O$ isotopes[44] and the corresponding equations for the vibrational isotope effect,[45] we obtained the value of 1442.3 cm^{-1} as an estimate of the $^{16}O^{18}O$ fundamental frequency in $^1\Delta_g$ state. Consequently, the calculated frequency of exciton-magnon-vibrational excitations of $^{16}O^{18}O$ molecules in $^1\Delta_g$ state is equal to 7988.3 $+1442.3=9430.6$ cm^{-1}, which practically coincides with the experimental frequency of maximum of the peak observed at 9430.3 cm^{-1}. In addition, we compared the integrated intensity of this isotope peak to the integrated intensity of the first exciton-vibron-magnon bound state of $^{16}O_2$ host crystal molecules. The ratio of these integrated intensities (0.005) coincides very well with the natural abundance of $^{16}O^{18}O$ isotope (0.004).[44] This is an additional strong evidence for the correctness of our assignment of the fine structure in spectra of α-O_2.

4. Singularities in spectra of exciton sidebands

Using the deconvolution procedure described above we reconstructed each of the sidebands involved in 0-0, 0-1, and 0-2 $^3\Sigma_g^-$-$^1\Delta_g$ electronic transitions. To obtain concrete assignment of peculiarities of electronic and electronic-vibrational sidebands we compared these spectra to a spectrum of directly measured phonon sideband to internal

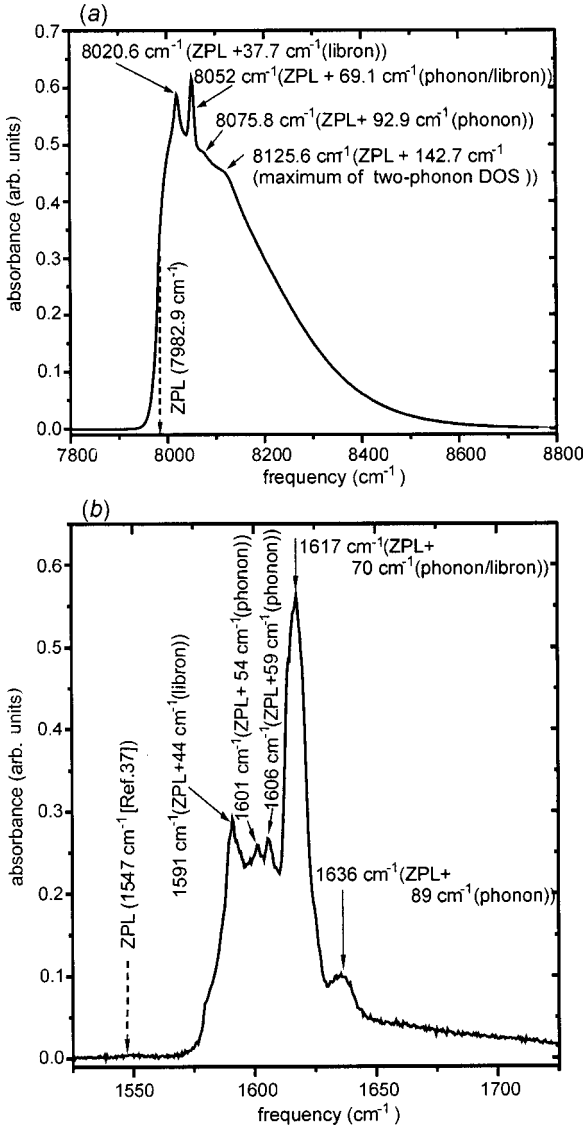

FIG. 4. Comparison of different kinds of phonon sidebands in α-O_2 ($T=11.2$ K): (a) sideband to electronic excitation $^3\Sigma_g^-(0)$-$^1\Delta_g(0)$ reconstructed by us (the ZPL frequency corresponds to the frequency of electronic excitations); (b) mid-ir spectrum of phonon sideband to fundamental vibrations (the ZPL frequency corresponds to the fundamental frequency).

vibrations in the mid-ir (see, e.g., Fig. 4). The frequencies of lattice excitations involved in the corresponding sideband were determined as the difference between the frequencies of the maxima in fine structure and the band-origin frequency ($^{16}O_2$ fundamental, electronic or electronic-vibrational transition). The comparison of these three kinds of sidebands shows that the frequencies of lattice excitations involved in electronic and electronic-vibrational sidebands agree quite well with the ones determined by analyzing vibrational sideband (see Fig. 4 and Table II). It is the second strong evidence for the correctness of our deconvolution procedure and of our interpretation of peculiarities in fine structure in spectra of electronic transitions.

The frequencies of the singularities in spectra of the vibrational sideband change very weakly with temperature in α-O_2, whereas only two maxima persist in β-O_2

TABLE II. Frequencies of distinctive maxima of fine structure in spectra of electronic absorption bands ($T=11.2$ K). Experimental inaccuracy is less than ± 1 cm^{-1}.

Transition	Peculiarities, (cm^{-1})	Assignment
$^3\Sigma_g^-$-$^1\Delta_g$(0-0)	7988.3	exciton-magnon bound state, $\mathbf{k}_1 \perp \mathbf{a}$, $k_1 \approx \pi/b$
	8003.7	exciton-magnon bound state, $\mathbf{k}_2 \perp \mathbf{b}$, $k_2 \approx \pi/a$
	8020.6	electronic excitation+libron (37.7 cm^{-1})
	8052	electronic excitation+phonon/libron (69.1 cm^{-1})
	8075.8	electronic excitation+phonon (92.9 cm^{-1})
	8125.6	electronic excitation+maximum of two-phonon DOS (142.7 cm^{-1})
$^3\Sigma_g^-$-$^1\Delta_g$(0-1)	9430.3	exciton-magnon-vibron (0-1) bound state of $^{16}O^{18}O$ isotope, $\mathbf{k}_1 \perp \mathbf{a}$, $k_1 \approx \pi/b$
	9471.1	exciton-vibron (0-1)-magnon bound state, $\mathbf{k}_1 \perp \mathbf{a}$, $k_1 \approx \pi/b$
	9480.8	exciton-vibron (0-1)-magnon bound state, $\mathbf{k}_2 \perp \mathbf{b}$, $k_2 \approx \pi/a$
	9500.6	electronic-vibrational (0-1) excitation+libron (32.2 cm^{-1})
	9538.6	electronic-vibrational (0-1) excitation+phonon/libron (70.2 cm^{-1})
$^3\Sigma_g^-$-$^1\Delta_g$(0-2)	10 933.4	exciton-vibron (0-2)-magnon bound state, $\mathbf{k}_1 \perp \mathbf{a}$, $k_1 \approx \pi/b$
	10 944.3	exciton-vibron (0-2)-magnon bound state, $\mathbf{k}_2 \perp \mathbf{b}$, $k_2 \approx \pi/a$
	10 959.9	electronic-vibrational (0-2) excitation+libron (35.7 cm^{-1})
$^3\Sigma_g^-$-$^1\Delta_g$(0-3)	12 364	exciton-vibron (0-3)-magnon bound state, $\mathbf{k}_1 \perp \mathbf{a}$, $k_1 \approx \pi/b$
$^3\Sigma_g^-$-$^3\Sigma_g^+$(0-0)	13 167	exciton (electronic excitation)
	13 223	exciton+libron (56 cm^{-1})
	13 304	exciton+maximum of two-phonon DOS (137 cm^{-1})
$^3\Sigma_g^-$-$^3\Sigma_g^+$(0-1)	14 582[a]	exciton-vibron (0-1)
	14 623	exciton-vibron (0-1)+libron (41 cm^{-1})
	14 703[a]	exciton-vibron (0-1)+maximum of two-phonon DOS (121 cm^{-1})

[a]Reference 21.

(fundamental-libron combination at 1591 cm^{-1} and fundamental-phonon one at 1617 cm^{-1},[13] i.e., the phonon DOS is hardly changed at the α-β phase transition. Figure 5 demonstrates the same behavior of the singularities of electronic (a) and electronic-vibrational (b) sidebands. This result provides the third strong confirmation of our assignment. The concrete frequency values of lattice excitations that caused these singularities slightly vary in spectra of the different kinds of phonon sidebands due to modification of the phonon DOS by modespecific interaction between the band origin (internal vibrations, electronic or electronic-vibrational excitations) and lattice excitations, according to our opinion. At higher temperatures (β-γ-liquid O_2), where the fine structure of sideband is smeared out, the difference between band maximum frequency and frequency of band origin (diamonds in Fig. 5) coincides with the frequency of the most intensive feature of sideband fine structure in α-O_2 (see Fig. 1, bottom), i.e., the maximum in electronic absorption bands in high-temperature phases is directly related to maximum of phonon DOS in these phases.

Our interpretation of electronic absorption bands as phonon sidebands to corresponding electronic excitations allows explaining consistently the spectra of $^3\Sigma_g^-$-$^1\Sigma_g^+$ transitions too. The distances between the band origins and the most intensive feature in these spectra in the α-O_2—about 60 cm^{-1} and 40 cm^{-1} in the (0-0) and (0-1) bands, respectively—correlate quite well with the ones in the spectra of the similar $^3\Sigma_g^-$-$^1\Delta_g$ transitions. Consequently, we assign these features in the $^3\Sigma_g^-$-$^1\Sigma_g^+$ spectra to the combinations of the corresponding high-energy excitations with libron modes (see Table II). Furthermore, we assign next features of the fine structure of these spectra, being 120–140 cm^{-1} away from the band-origin frequencies, to the maxima of two-phonon DOS, similarly to the ones in the $^3\Sigma_g^-$-$^1\Delta_g$ spectra.

C. From spectra to magnetism and phase transitions

1. Frequencies of electronic transitions to probe a long-range magnetic order in solid oxygen

The most important information obtained by our deconvolution procedure concerns the temperature behavior of the frequencies of the pure electronic and electronic-vibrational transitions (Fig. 6). The greatest statistical error in determining these values was in the α phase but did not exceed 1.5, 5,

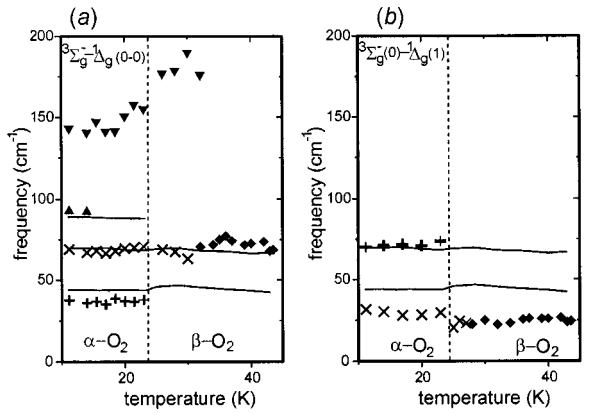

FIG. 5. Peculiarities of fine structure belonging to $^3\Sigma_g^-(0)$-$^1\Delta_g(0)$ electronic (a) and $^3\Sigma_g^-(0)$-$^1\Delta_g(1)$ electronic-vibrational sidebands (solid lines show the same for the main maxima of sideband to fundamental vibrations). The frequencies of peculiarities (plus, cross, up and down triangle) are calculated relatively to corresponding band origin frequency. Diamonds show the difference between band maximum frequency and frequency of the band origin [see Fig. 2(d)]. The assignment of peculiarities is given in Fig. 4.

and 10 cm^{-1} for $^3\Sigma_g^-(0)$-$^1\Delta_g(0)$, $^3\Sigma_g^-(0)$-$^1\Delta_g(1)$ excitations and frequency of simultaneous excitation of $^3\Sigma_g^-(0)$-$^1\Delta_g(0)$ exciton plus $^3\Sigma_g^-$(0-1) vibron, respectively. It is interesting to note that the theoretical estimate of the $^3\Sigma_g^-(0)$-$^1\Delta_g(0)$ excitation frequency in the α-O_2 (7971.4 cm^{-1}) (Ref. 29) is in a qualitative agreement with our values drawn directly from experimental data. The temperature behavior of the frequency of all three kinds of electronic excitations is qualitatively similar: (i) very weak changes in the range from 24 to 87 K in comparison with a substantially stronger temperature dependence in α-oxygen; (ii) absence of observable changes at melting point; (iii) very small jump in frequency (a few cm^{-1}) at β-γ phase transition in comparison to very big jump (80–90 cm^{-1}) at α-β phase transition.

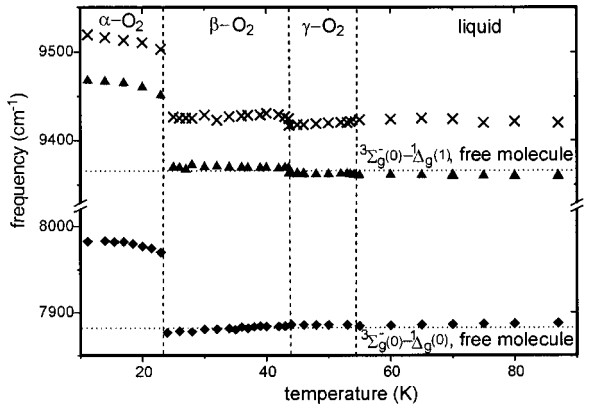

FIG. 6. Temperature dependence of frequencies of the following excitations: $^3\Sigma_g^-(0)$-$^1\Delta_g(0)$ electronic (diamond), $^3\Sigma_g^-(0)$-$^1\Delta_g(1)$ electronic-vibrational (triangle), simultaneous excitation of $^3\Sigma_g^-(0)$-$^1\Delta_g(0)$ exciton and $^3\Sigma_g^-$(0-1) vibron (cross).

It is known,[3,19,20] that intermolecular interaction between two oxygen molecules consists of two components—Van der Waals forces and spin-spin interaction [$-2J\mathbf{S}_1\mathbf{S}_2$, where J and $\mathbf{S}_i$ ($i=1, 2$) are Heisenberg exchange constant and spin of ith molecule, respectively]. Because of very small quadrupole moment of oxygen molecule a contribution to the intermolecular forces due to an electrostatic interaction can be neglected.[7] Very small changes in the frequencies of the electronic and electronic-vibrational transitions in high-temperature magnetic disordered phases ($T=24-87$ K) as well as during structural phase transitions accompanied by big volume changes (4.2% at melting point and 5.4% at β-γ phase transition) indicate that these characteristics of electronic excitations are hardly influenced by Van der Waals interaction in contrast to the behavior of band maxima [Fig. 2 (d)]. Therefore, the big jump in frequencies of electronic transitions at α-β phase transition is completely caused by the appearance of long-range magnetic order in α-O_2 and reflects a difference in exchange field between these two phases.

Taking into account an interaction (J_{nn}) between four nearest neighbors in α phase only and neglecting short-range magnetic order in β-O_2, we obtain the following estimate of a change in exchange field at α-β phase transition:

$$\Delta U = -8J_{nn}\langle \mathbf{S}_1\mathbf{S}_2\rangle \tag{3}$$

In our approximation, the expression (3) corresponds to an exchange field U_α in α-oxygen at the α-β phase transition point. An increase in the frequency of electronic excitations in the α-O_2 lowering temperature (see Fig. 6) is caused by strengthening the exchange constant J_{nn} due to a decrease in the intermolecular distance as well as due to an increase in the magnetic order parameter σ. The temperature-caused changes in the frequency of electronic transition (as well as in the electronic-vibrational one) within the α phase are relatively small in comparison to the jump in frequency at α-β phase transition. It means that a Neel point for a two-sublattice antiferromagnetic structure of α-oxygen is lying substantially higher than the temperature of α-β phase transition in agreement with results obtained measuring magnetic susceptibility in high magnetic fields directly.[46] Then $\langle \mathbf{S}_1\mathbf{S}_2\rangle \cong -\sigma^2$ and therefore

$$U_\alpha = 8J_{nn}\sigma^2 \tag{4}$$

Applying this expression to the experimentally determined jump in frequency of electronic excitations $^3\Sigma_g^-(0)$-$^1\Delta_g(0)$ (93.6 cm^{-1}) and using the value of relative intensity of magnetic (101) diffraction peak (about 0.65) as an estimate of the value of σ^2,[47] we obtain $J_{nn}=18$ cm^{-1} in α-O_2 near the α-β phase transition. Our value agrees quite well with the result of *ab intio* calculations for the same value of intermolecular distance: $J_{nn}=20.8$ cm^{-1} (Ref. 48). This very good quantitative agreement strongly supports our explanation of the origin of the jump in the frequency of the pure electronic (as well as electronic-vibrational) transition $^3\Sigma_g^-$-$^1\Delta_g$ at the α-β phase transition due to an appearance of the long-range magnetic order in the α-O_2. Therefore, the

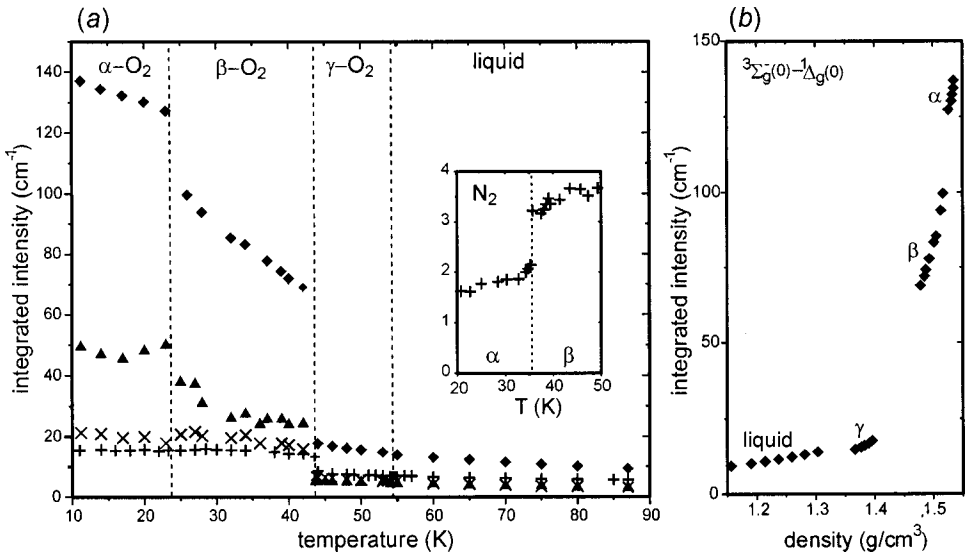

FIG. 7. (a) Temperature dependences of integrated intensity of Stokes component of different kinds of phonon sidebands in condensed oxygen: $^3\Sigma_g^-(0)$-$^1\Delta_g(0)$ electronic side-band (diamond), $^3\Sigma_g^-(0)$-$^1\Delta_g(1)$ electronic-vibrational sideband (triangle), sideband to simultaneous excitation of $^3\Sigma_g^-(0)$-$^1\Delta_g(0)$ exciton plus $^3\Sigma_g^-(0\text{-}1)$ vibron (cross), sideband to fundamental vibrations (plus). Inset shows the same for the sideband to fundamental vibrations in solid nitrogen. (b) Integrated intensity of Stokes component of $^3\Sigma_g^-(0)$-$^1\Delta_g(0)$ electronic sideband as function of density.

electronic absorption bands can be successfully used to probe magnetic order in high-pressure phases of oxygen where this information is absent. Furthermore, the value of the jump in the frequency of electronic excitations at a magnetic order-disorder phase transition can be utilized to estimate the Heisenberg exchange constant in these phases.

2. Integrated intensity of the phonon sidebands: physical mechanism of combined excitations in oxygen

In general, two factors cause changes in the total integrated intensity of any phonon-sideband varying temperature: (i) raising a contribution of the ''anti-Stokes'' component as temperature increases and (ii) changes in the absorbance due to temperature-caused variations in crystal (intermolecular interaction; translational, orientational, and magnetic order parameters; coupling between band origin excitation and lattice ones, etc.). Since we are interested here only in the second physical mechanism, we divided the spectra of phonon sidebands into ''Stokes'' and ''anti-Stokes'' components and integrated their ''Stokes'' part. Temperature dependences of integrated intensity of ''Stokes'' component of phonon sidebands involved in 0-0 and 0-1 electronic transitions as well as of the oxygen vibron sideband are presented in Fig. 7(a). In liquid and γ-oxygen all kinds of sidebands show qualitatively similar temperature dependence—integrated intensity increases lowering temperature slightly. No discontinuity is observed at melting point similarly to the behavior of frequencies of band origin (Fig. 6). Both electronic and vibrational sidebands show clearly a discontinuity in the integrated intensity at γ-β phase transition unlike the behavior of frequencies of the electronic and electronic-vibrational transitions.

Then below the $\gamma \rightarrow \beta$ phase transition all four sidebands show different temperature behavior [Fig. 7(a)] and can be divided into two groups: (1) $^3\Sigma_g^-(0)$-$^1\Delta_g(0)$ electronic (diamonds) and $^3\Sigma_g^-(0)$-$^1\Delta_g(1)$ electronic-vibrational sidebands (up triangles); (2) band corresponding to simultaneous excitation of $^3\Sigma_g^-(0)$-$^1\Delta_g(0)$ exciton plus $^3\Sigma_g^-(0\text{-}1)$ vibron (crosses) as well as sideband to fundamental vibrations (pluses). The integrated intensity of electronic and electronic-vibrational sidebands increases lowering temperature and possesses a clear jump at α-β phase transition. Whereas the integrated intensities of sidebands belonging to second group show very weak temperature dependence in these phases and are almost insensitive to the α-β phase transition. In general, the integrated intensity of a sideband is proportional to the coupling between internal molecule excitations and lattice excitations multiplied by the phonon DOS. Since phonon DOS is the same for all four sidebands, one may conclude that the coupling mechanism is different for two groups. The interaction between internal vibrations and lattice phonons is mainly responsible for the absorbance in the second group of transitions, whereas the interaction between electronic excitations and lattice phonons plays the most important role for the absorbance in the first group of transitions.

Usually (see, e.g., Ref. 38), ir absorption due to additive high-order processes raises increasing temperature because of an increase in occupation of excited phonon states [see, e.g., Eq. (1a)]. However, all kinds of sidebands in condensed oxygen show opposite temperature behavior. To prove if this is a special property of oxygen we carefully recorded the phonon sideband to the $^{14}N_2$ fundamental in pure nitrogen crystals (mid-ir, 2200–2700 cm^{-1}). The experimental setup as well as the nitrogen crystal growing procedure are described elsewhere.[37] The temperature dependence of the integrated intensity of Stokes component of phonon sideband

to the nitrogen fundamental is shown in the insert in Fig. 7(a). Comparing the oxygen case [pluses in Fig. 7(a)] to the nitrogen case [insert in Fig. 7(a)] we find that (i) the nitrogen combination band is by more than one order of magnitude less intense; (ii) the temperature behavior of the integrated intensity of nitrogen sideband qualitatively follows Eq. (1a); (iii) the phase transition from orientationally ordered α-N_2 to orientationally disordered β-N_2 causes a positive jump in integrated intensity, whereas the $\beta \rightarrow \gamma$ phase transition in solid O_2 causes a negative jump. If we consider the behavior in N_2 to be the usual case, we introduce the spin-spin interaction in oxygen to explain all three deviations from the normal situation, mentioned above. It is known[36] that the vibrational sideband in α-N_2 derives its intensity from optical anharmonicity, i.e., off-diagonal elements in polarizability, whereas mechanical anharmonicity (i.e., vibration-phonon coupling through anharmonicity of vibrational potential) is negligible. Since the polarizabilities of N_2 and O_2 molecules do not differ significantly,[49] a contribution to the intensity of combination bands due to optical anharmonicity in oxygen is expected to be of the same order of magnitude as in N_2 crystal. Consequently, the phonon sidebands in solid oxygen derive their intensity mainly from an anharmonicity of intermolecular interaction. Due to a strong dependence of exchange interaction on orientational and translational motion of oxygen molecules,[48] an interaction between electronic (or vibrational) excitations and lattice phonons is assisted by spin-spin interaction. This additional specific interaction explains why all kinds of combination bands in condensed oxygen are stronger in comparison to other molecular crystals. And this effect must be stronger in orientationally ordered phases due to substantially stronger coupling between spin and other degrees of freedom of O_2 molecules. Consequently, two key structural factors must influence the intensity of a combination band:density and degree of orientational order. Figure 7(b) confirms these general statements directly (to rescale temperature into density the data from Refs. 3 and 50 were used). The integrated intensity $I_{\mathrm{int}}(\rho)$ raises increasing density, i.e., larger spin-spin interaction. This dependence is characterized by a gentle slope in the region of orientationally disordered phases (liquid and γ-oxygen) in contrast to a steep slope in the orientationally ordered β- and α-O_2; these slopes in α-O_2 and β-O_2 are insignificantly different.

3. Magnon excitations in α-O_2

In this section, we will determine the magnon frequencies at Brillouin zone boundaries analyzing our spectra. We used the theoretical results from Ref. 34 to determine a direction of propagation of combined exciton-magnon excitations.

The general formulas for the frequencies of electronic and electronic-vibrational excitations in crystal can be written as following:

$$\omega_{0\text{-}v}^{\mathrm{exc}}(\mathbf{k}) = \omega_{0\text{-}v}^{\mathrm{gas}} + \Delta\omega_{0\text{-}v}^{\mathrm{env}} + \Delta\omega_{0\text{-}v}^{\mathrm{res}}(\mathbf{k}), \quad v = 0,1,\ldots. \tag{5}$$

Here v is the vibrational quantum number, $\omega_{0\text{-}v}^{\mathrm{gas}}$ is the value of the frequency of 0-v electronic-vibrational transition in the free molecule; $\Delta\omega_{0\text{-}v}^{\mathrm{env}}$ and $\Delta\omega_{0\text{-}v}^{\mathrm{res}}(\mathbf{k})$ are environmental and resonance frequency shifts due to intermolecular interaction in the crystal. The expressions (5) for the frequencies of electronic excitations have the same form as ones in case of vibron frequencies.[39] Similarly to vibron modes,[51] the terms $\Delta\omega_{0\text{-}v}^{\mathrm{env}}$ and $\Delta\omega_{0\text{-}v}^{\mathrm{res}}$ $(\mathbf{k})$ include a renormalization of exciton (or exciton-vibron) frequencies by quasiparticle interactions: exciton-libron, exciton-magnon, etc. The resonance term describes the spread of an electronic level into a quasicontinuous energy band due to an exchange of excitations between molecules in crystal. According to our interpretation (see Sec. III B.I), the band origin frequencies (as ZPL) correspond to the frequencies of an excitation of the single molecules in crystal, i.e., the resonance term does not have to be included in these values:

$$\omega_{0\text{-}v}^{\mathrm{ZPL}} = \omega_{0\text{-}v}^{\mathrm{gas}} + \Delta\omega_{0\text{-}v}^{\mathrm{env}} \tag{6}$$

Putting expression (6) into (5) and equating frequencies of exciton-magnon (or exciton-vibron-magnon) bound states to sum of exciton (or exciton-vibron) and magnon ones we obtain the following system of equations linking frequencies of all excitations observed in our experiment together:

$$\omega_{0\text{-}v}^{\mathrm{exc\text{-}mag}}(\mathbf{k}_i) = \omega_{0\text{-}v}^{\mathrm{ZPL}} + \Delta\omega_{0\text{-}v}^{\mathrm{res}}(\mathbf{k}_i) + \omega_{\mathrm{mag}}(\mathbf{k}_i). \tag{7}$$

$\omega_{\mathrm{mag}}(\mathbf{k}_i)$ are the magnon frequencies at Brillouin zone boundaries $(i=1,2;\ \mathbf{k}_1 \perp \mathbf{a},\ \mathbf{k}_1 \approx \pi/\mathbf{b};\ \mathbf{k}_2 \perp \mathbf{b},\ \mathbf{k}_2 \approx \pi/\mathbf{a})$. In Eq. (7), we neglected an additional frequency shift of exciton-magnon (or exciton-vibron-magnon) bound states due to creation of these states, which is expected to be small.

Two terms contribute to an environmental frequency shift of an electronic-vibrational state—a shift $\Delta\omega_{0\text{-}0}^{\mathrm{env}}$ due to an electronic excitation and a shift $\Delta\omega_{v}^{\mathrm{env}}$ due to a subsequent vibrational excitation:

$$\Delta\omega_{0\text{-}v}^{\mathrm{env}} = \Delta\omega_{0\text{-}0}^{\mathrm{env}} + \Delta\omega_{v}^{\mathrm{env}}. \tag{8}$$

It can be shown,[51] that the environmental and resonance shifts of high-excited vibrations states can be expressed in terms of corresponding values for the fundamental vibrations:

$$\Delta\omega_{v}^{\mathrm{env}} \equiv v\,\Delta\omega_{0\text{-}1}^{\mathrm{env}}, \quad \Delta\omega_{0\text{-}v}^{\mathrm{res}} \sim (x_e)^{v\text{-}1}\Delta\omega_{0\text{-}1}^{\mathrm{res}} \quad \text{for } v \geqslant 1 \tag{9}$$

x_e is anharmonic constant of the free molecule. Since x_e is very small $(x_e^{O_2} < 10^{-2})$,[1] the contribution of the resonance shift to the exciton-vibron frequencies can be neglected for any vibrational excitations with vibrational quantum number higher than 1. Applying these theoretical results to Eq. (7), we obtain the closed system of equations to determine the magnon frequencies at Brillouin zone boundaries as well as the environmental and resonance frequency shifts of electronic and electronic-vibrational states directly from the experimental data (Tables I and II). All results obtained collected in Table III. Two facts are remarkable: the frequency shift of electronic-vibrational transitions in the α-O_2 is

TABLE III. Parameters of energy spectrum of $^3\Sigma_g^-(0)$-$^1\Delta_g$ excitations ($T=11.2$ K) as well as magnon frequencies at boundaries of Brillouin zone drawn from experimental results (for details see text).

Quantity	*k*-space point	Value (cm^{-1})
$\Delta\omega_0^{env}$		100.3
$\Delta\omega_{0\text{-}1}^{env}$		0.6
$\Delta\omega_{0\text{-}0}^{res}$	$\mathbf{k}\perp\mathbf{a}$, $k\approx\pi/b$	−3.6
$\Delta\omega_{0\text{-}0}^{res}$	$\mathbf{k}\perp\mathbf{b}$, $k\approx\pi/a$	0.95
$\Delta\omega_{0\text{-}1}^{res}$	$\mathbf{k}\perp\mathbf{a}$, $k\approx\pi/b$	−4.8
$\Delta\omega_{0\text{-}1}^{res}$	$\mathbf{k}\perp\mathbf{b}$, $k\approx\pi/a$	−6.1
ω_{mag}	$\mathbf{k}\perp\mathbf{a}$, $k\approx\pi/b$	9.0
ω_{mag}	$\mathbf{k}\perp\mathbf{b}$, $k\approx\pi/a$	19.9

mainly caused by electronic excitation of oxygen molecule ($\Delta\omega_{0\text{-}0}^{env}\gg\Delta\omega_v^{env}$); the dispersion of the exciton-vibron excitations ($\Delta\omega_{0\text{-}1}^{res}$) is comparable to the exciton one ($\Delta\omega_{0\text{-}0}^{res}$).

The magnon energy values at Brillouin-zone boundaries estimated by us (9.9 and 19.9 cm^{-1}) are close to those at zone center[14,16] (6.4 and 27.2 cm^{-1}) and are significantly different from the estimate obtained by Litvinenko *et al.*[55] ($\approx$38 cm^{-1}). The last derived this value by simple equating the shift of band maximum[56] of $^3\Sigma_g^-\rightarrow{}^1\Delta_g$ and some double transitions, caused by the α-β phase transformation [or by introducing nonmagnetic impurity (10–20 %N_2) in α-O_2], to the energy of one or two magnon excitations at zone boundary, i.e., these authors considered ir-active optical bands in the α-O_2 as exciton-magnon bands (plus some phonon excitations). Shortcomings of this interpretation were already stated in Sec. III B. In fact, the displacement of the optical bands as a whole toward lower frequency at the α-β phase transition reflects changes in the frequency of the electronic (or electronic-vibrational) excitations due to the radical reconstruction of the crystal ground state at this transition. Noteworthy, the 20 cm^{-1} vibrations were found out by careful analysis of the fine structure of the electronic-vibrational bands of $2^3\Sigma_g^-\rightarrow 2^1\Delta_g$ series at 1.3 K and tentatively assigned to magnon excitations.[57] Since the previous theoretical calculations of the magnon energy spectra $\omega_{mag}(\mathbf{k})$ were based on the value of 38 cm^{-1} (Ref. 18) or twice it (Ref. 3) as an estimate of the magnon frequency at Brillouin zone boundary, new theoretical investigations are necessary.

To explore the temperature behavior of spin excitations at boundaries of the Brillouin zone we solved the system of equations (7) at different temperatures using the experimental temperature dependences of the frequencies of exciton (exciton-vibron)-magnon bound states [Fig. 8(a)] and of the band origin ones (Fig. 6) and determined the corresponding magnon frequencies [Fig. 8(b)]. While the frequency of magnons propagating in *a* direction shows a weak trend to decrease with increasing temperature, the frequency of magnons propagating along the monoclinic axis possesses a characteristic minimum at about 17 K, which coincides with the maximum in temperature dependence of *b* lattice parameter.[3] Therefore, the temperature behavior of magnon

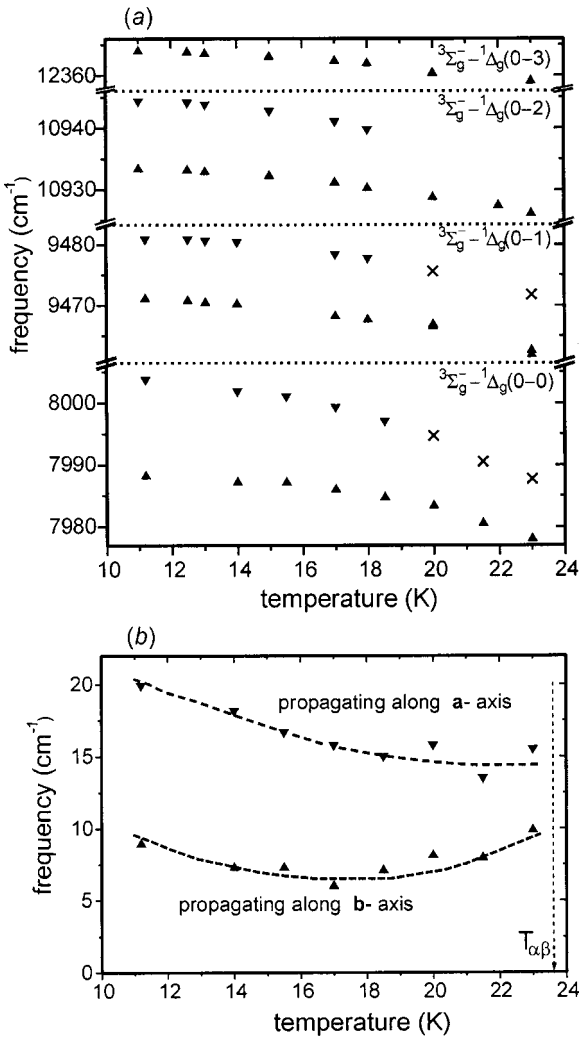

FIG. 8. Temperature dependence of frequency of: (a) exciton (exciton-vibron)-magnon bound states (crosses are the values found out by modeling experimental spectra); (b) magnons at boundaries of Brillouin zone (lines, guide to the eye).

frequencies at Brillouin zone boundaries mainly reflects the thermal expansion of the basal plane of α-O_2 crystal. Figure 8(b) also shows that no considerable softening of magnon frequencies is observed to be approaching the α-β phase transition, i.e., magnetic disordering is not a precursor to this transition. This principal conclusion drawn by us directly from experimental spectroscopic data agrees with results of neutron diffraction studies,[6(b)] where no considerable changes in spin ordering were observed at 22 K in comparison to 6 K, as well as of Monte Carlo simulations of α and β phases.[52]

4. Order and nature of α-β phase transition

The clear jump in electronic and electronic-vibrational frequencies at α-β phase transition (Fig. 6) indicates that this transition is being of *first* order. To obtain additional direct experimental proofs of this principal statement we carefully monitored the behavior of $^3\Sigma_g^-$-$^1\Delta_g$ electronic absorption

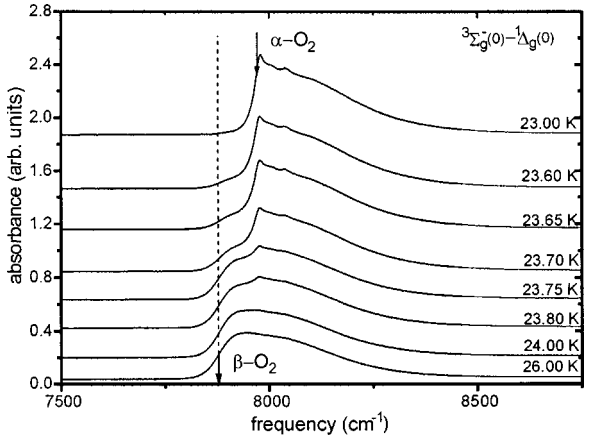

FIG. 9. Temperature evolution of the $^3\Sigma_g^-{}^1\Delta_g(0\text{-}0)$ spectra near to the $\beta\rightarrow\alpha$ phase transition (cooling). The solid and dotted arrows indicate the frequencies of the electronic excitations in the α and β phases. The superposition of the electronic sidebands related to the α- and β-O_2, i.e., coexistence of the α and β phases, is clearly visible.

bands in the vicinity of this phase transition. Figure 9 shows the spectra of $^3\Sigma_g^-$-$^1\Delta_g(0\text{-}0)$ electronic transition by cooling one of our samples. The coexistence of α and β phases is clearly visible in the temperature range from 23.8 K to 23.6 K. The coexistence of α and β phases is also observed by warming our samples, i.e., during the $\alpha\rightarrow\beta$ phase transition, at a bit higher temperatures in comparison to the $\beta\rightarrow\alpha$ phase transition. Two-phase region was also observed by us in spectra of all electronic-vibrational bands.

To be sure that these principal results reflect inherent properties of oxygen crystal and are not caused by possible temperature gradients in our sample—due to cryostat geometry or heating by irradiation—we compared our results of different samples and various optical geometries. Since the two-phase region in our spectra were observed in the same temperature regions in all cases, we are convinced to observe the true phase coexistence during phase transition. It is the second direct experimental proof that the α-β phase transition is definitely of the first order for studying electronic absorption bands.[53]

The drastic changes in the electronic spectra observed by us (Figs. 6 and 9) at the α-β phase transition seem contradicting to the high-accuracy x-ray structural data,[3] according to them this phase transition is accompanied by very small changes in molar volume. These authors explained this behavior in terms of regular thermal expansion of crystal. Consequently, they classified this phase transition as ''mostly second order.'' To solve this discrepancy we reanalyzed and reinterpreted the data on the temperature dependence of lattice parameters presented in Ref. 3.

To compare the structures of α and β phases we considered the structural unit cell of β-O_2 in monoclinic axes following Ref. 3. We introduced three specially selected structural parameters to describe uniformly changes in structure of both phases: area S of unit cell in basal plane [$S_{\alpha\text{-}O_2}=a\cdot b$, $S_{\beta\text{-}O_2}=R^2\sqrt{3}$, R is the distance between the nearest

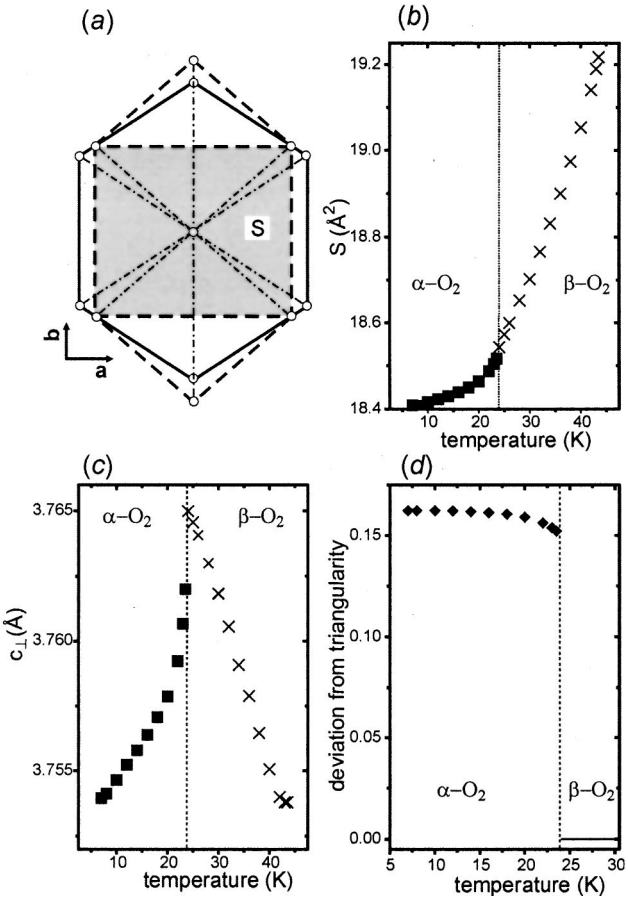

FIG. 10. Changes in structure of α- and β-O_2 vs temperature (our reanalysis of the structural data from Ref. 3): (a) picture of the basal plane of α- (dashed lines) and β- (solid lines) O_2, (b) area of unit cell in basal plane, (c) interplane separation, (d) deviation from triangularity in basal plane ($\delta=\sqrt{3}-a/b$). Solid line (d) marks zero deviation from triangularity in β-O_2 for comparison to α-O_2 data.

neighbors in the β-O_2 see Fig. 10(a)], interlayer separation $c_\perp$ and the deviation from triangularity in the basal plane δ [$\delta_{\alpha\text{-}O_2}=\sqrt{3}-a/b$; $\delta_{\beta\text{-}O_2}$ equals zero by definition, see Fig. 10(a)]. The temperature dependences of these parameters are presented in Figs. 10(b)–10(d). It can be seen that no discontinuity in the area of unit cell in basal plane is observed at the α-β phase transition [Fig. 10(b)], while the changes in the $c_\perp$ parameter are very small [about 0.003 Å, Fig. 10(c)]. These facts—an absence of discontinuity in the area of unit cell in basal plane and very small changes in the interplane distance (less than 0.1%)—explain difficulties to classify the order of the α-β phase transition by analyzing changes in molar volume only. Figure 10(d) shows what actually happens at this transition: *the very strong distortion of the basal plane arises by a sudden deviation from triangularity* ($\delta|_{T_{\alpha\beta}}\approx 0.15$), i.e., the *correct* selection of the structure characteristics being analyzed provides *conclusive* proof that the α-β phase transition is of first order.

Our next objective is to clear up the nature of this phase transition, which has been under discussion for more than three decades. There is a common opinion that an increase in

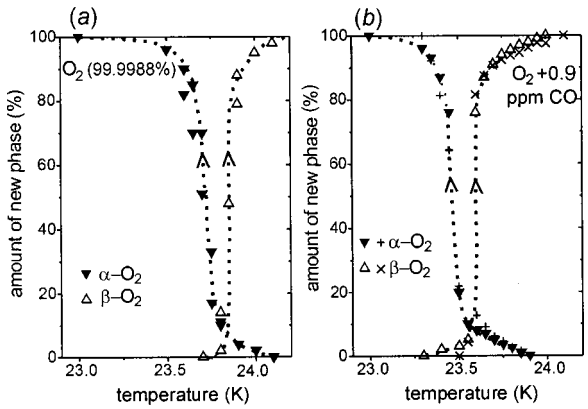

FIG. 11. Kinetics of the α-β phase transition investigated by monitoring the $^3\Sigma_g^-$-$^1\Delta_g(0\text{-}0)$ spectra: (a) relative amount of new phase as a function of temperature (oxygen 99.998%); (b) the same as in (a) for oxygen (99.998%) enriched by 0.9 ppm CO (crosses mark the normalized integrated intensity of the CO fundamental from Ref. 13). The dashed lines serve as a guide to the eye. The arrows indicate a direction of the thermal process—cooling (the $\beta \rightarrow \alpha$ transition) and warming (the $\alpha \rightarrow \beta$ transition).

temperature leads to some instability of the α-O_2 crystal phase having either purely magnetic[11] or magnetoelastic origin.[12] We have already shown in the previous section that the temperature-caused changes in magnetic subsystem of the α-O_2 cannot be considered as a precursor of the $\alpha \rightarrow \beta$ phase transition, i.e., a purely magnetic origin of this transition must be excluded. The data presented in Figs. 10 show that no structure instability is observed approaching the α-β phase transition. Indeed, the temperature-caused changes in the deviation from triangularity in basal plane $\Delta\delta(T) = \delta(T) - \delta(0)$ [see Fig. 10 (d)], which is the only quantity relevant to the principal structure changes occurring during this phase transition, are about 0.01 in the whole temperature range of α-O_2 ($T < 24$ K), i.e., $\Delta\delta(T)/\delta|_{T_{\alpha\beta}} \approx 6\,\%$. Therefore, a magnetoelastic origin of the α-β phase transition must be ruled out as well.

All these spectroscopic and structural results allow us to draw the conclusion that the α-β phase transition is caused by simple competition between the free energies of two possible structures of solid oxygen—the elongated triangular crystal structure possessing the two-sublattice antiferromagnetic order (α-O_2) and the ideal triangular structure with a short-range (or dynamic)[54] magnetic order (β-O_2).

5. Kinetics of the α-β phase transition

To explore the kinetics of the α-β phase transition we divided each of the spectra in the two-phase region (Fig. 9) into two components—bands related to α- and to β-O_2—and normalized their integrated intensities to the one of the total spectrum (100%) [Fig. 11(a)]. If we define the temperature point, which corresponds to 50% of a transformation as the temperature of this transition, a clear hysteresis is observed for the α-β phase transition: $T^{50\%}_{\alpha\rightarrow\beta} - T^{50\%}_{\beta\rightarrow\alpha} \approx 0.15$ K. In addition, the transition at warming ($T_{\beta\rightarrow\alpha}$) begins at a little lower temperature than the transition at cooling ($T_{\beta\rightarrow\alpha}$). According to our previous investigations, our samples of solid oxygen contain about 40 ppb of CO as a natural contamination of the original gas.[13] Consequently, the small splitting of the α-β phase transition [cooling-warming paths in Fig. 11(a)] could be, in principle, explained by a known splitting of phase transition in binary systems (O_2-CO in our case). To check this explanation we studied the samples specially enriched by CO (O_2+0.9 ppm CO) The results are [Fig. 11(b)]: (i) the cooling and warming curves are shifted toward lower temperatures; (ii) the splitting of the α-β phase transition becomes more pronounced. To be convinced that these results are not connected to some specific properties of electronic absorption spectra we added to Fig. 11(b) by crosses the data from Ref. 13 obtained by monitoring spectra of the fundamental of CO molecules matrix isolated in solid oxygen/(mid-ir region). Both sets of data coincide very well. Moreover, as it was shown[13] the CO molecules dissolved in solid oxygen influence the β-γ phase transition too. It means that the phase transitions in solid oxygen are indeed extremely sensitive to small concentrations of CO impurities. Preliminary results of FTIR studies of oxygen enriched by N_2 show that nitrogen molecules influence the α-β phase transition of oxygen weaker than CO but in a similar manner. The smearing of the α-β phase transition in oxygen due to very small concentrations of impurities can be the reason for discrepant results by different groups, performing structural or calorimetric investigations, tried to characterize the order of this transition.

IV. CONCLUSION

The temperature behavior of $^3\Sigma_g^-$-$^1\Delta_g$ absorption bands of oxygen was systematically investigated by spectroscopy studies (FTIR, 7000–15 000 cm^{-1}) in the temperature range from 10 K to 90 K at ambient pressure. Due to excellent optical quality of our crystal samples, we were able to investigate in details electronic-vibrational excitations (up to vibrational number 3) as well as a complex fine structure of spectra. For comparison, we also studied the phonon sideband to internal vibration in solid O_2 and N_2 (mid-ir, 800–3000 cm^{-1}).

We interpret these electronic absorption bands as phonon sidebands to electronic or electronic-vibrational excitations plus (in magnetic ordered phases) exciton (-vibron)-magnon bound states; therefore, the singularities in spectra of these sidebands are related to maxima of the phonon DOS similarly to the ones in the phonon sideband to internal vibrations (''vibron'' sidebands). A special procedure to analyze the band shape of electronic spectra was worked out to determine the frequencies of electronic and electronic-vibrational excitations (as ZPI). Using this procedure, we found the frequencies of electronic and electronic-vibrational excitations ($^3\Sigma_g^-$-$^1\Delta_g$) in condensed oxygen and explored their temperature behavior in temperature range from 10 K to 90 K. We discovered that the frequency shift of electronic excitations in condensed oxygen is mainly governed by magnetic order and hardly ruled by changes in molar volume. Therefore, this kind of spectroscopy can be used to probe indirectly magnetic order in high-pressure phases, where direct

information is absent up to now. A joint analysis of different kinds of excitations in α oxygen allowed us to determine the magnon frequencies at boundaries of the Brillouin zone as well as to explore their temperature behavior.

Based on a comparative analysis of the integrated intensity of different kinds of phonon sidebands, we are able to conclude that an interaction between the intramolecular and lattice excitations is assisted by an exchange interaction in condensed oxygen. Even more generally, we speculate that all kinds of combined excitations are exchange interactions assisted in solid oxygen. This general statement can be directly proved by further spectroscopic investigations of other kinds of combined excitations such as two-libron, libron-phonon, two-vibron, etc.

We obtained several unambiguous direct experimental proofs that the α-β phase transition is of *first order*. Any considerable softening of magnon frequencies is not observed approaching the α-β phase transition. Our own reanalysis of structural data by others showed that the temperature-caused changes in the structure of α-oxygen cannot be considered as a precursor of the α-β phase transition. Therefore, we think that the α-β phase transition is a usual phase transition of first order, whose concrete temperature point is determined by equating the free energy of monoclinic magnetically ordered α-phase to the free energy of rhombohedral structure of β-O_2 with short-range triangular antiferromagnetic ordering.

Our precise investigation of the kinetics of the α-β phase transition showed that a smearing of this transition is observed even at concentrations of impurities as small as 1 ppm. This fact can serve as an obvious explanation for the contradictions in literature (results drawn by different investigators) concerning the order of the α-β phase transition in solid oxygen.

ACKNOWLEDGMENTS

This work was supported by Deutsche Forschungsgemeinschaft (Grant No. Jo 86/10-1). S.A.M. acknowledges support by Gottlieb Daimler-und Karl Banz-Stiftung. One of us (H.J.J.) is grateful for the support of the Department of Chemistry, University of Florence, Italy. We appreciate the help of M. Minenko and M. Vetter during the initial stages of experiments as well as the valuable discussions with V. Loktev, J. Kreutz, L. Ulivi, M. Santoro, and R. Bini.

[1] P. H. Krupenie, J. Phys. Chem. Ref. Data **1**, 423 (1972); T. G. Slanger and P. C. Cosby, *ibid.* **92**, 267 (1988).

[2] M. Nicol, K. R. Hirsch, and W. B. Holzapfel, Chem. Phys. Lett. **68**, 49 (1979); M. Nicol and K. Syassen, Phys. Rev. B **28**, 1201 (1983).

[3] I. N. Krupskii, A. I. Prokhvatilov, Yu. A. Freiman, and A. I. Erenburg, Fiz. Nizk. Temp. **5**, 271 (1979) [Sov. J. Low Temp. Phys. **5**, 130 (1979)].

[4] D. E. Cox, E. J. Samuelssen, and K. H. Beckurts, Phys. Rev. B **7**, 3102 (1973); F. Leoni and F. Sacchetti, *ibid.* **7**, 3112 (1973); F. Dunstetter, O. Hardouin Duparc, V. P. Plakhty, J. Schweizer, and A. Delapalme, Fiz. Nizk. Temp. **22**, 140 (1996) [Low Temp. Phys. **22**, 101 (1996)].

[5] M. F. Collins, Proc. Phys. Soc. London **89**, 415 (1966).

[6] (a) R. A. Alikhanov, Zh. Eksp. Teor. Fiz., Pis'ma Red. **5**, 430 (1967) [JETP Lett. **5**, 349 (1967)]; (b) R. J. Meier and R. B. Helmholdt, Phys. Rev. B **29**, 1387 (1984).

[7] A. P. Brodynaski and Yu. A. Freiman, Fiz. Nizk. Temp. **11**, 436 (1985) [Sov. J. Low Temp. Phys. **11**, 231 (1985)].

[8] C. H. Fagerstroem and A. C. Hollis-Hallet, J. Low Temp. Phys. **1**, 3 (1969).

[9] L. Lipinski, A. Szmirka-Grzebyk, and H. Manuszkiewicz, Cryogenics **36**, 921 (1996); J. Low Temp. Phys. **111**, 399 (1998).

[10] J. M. Dundon, Phys. Lett. **61A**, 58 (1977); E. Domany and E. K. Riedel, Phys. Rev. Lett. **40**, 561 (1978).

[11] V. A. Slyusarev, Yu. A. Freiman, and R. P. Yankelevich, Pis'ma Zh. Eksp. Teor. Fiz **30**, 292 (1979) [JETP Lett. **30**, 270 (1979)]; Fiz. Nizk. Temp. **6**, 219 (1980) [Sov. J. Low Temp. Phys. **6**, 105 (1980)]; 536 (1981) [**7**, 265 (1981)].

[12] Yu. B. Gaididei and V. M. Loktev, Fiz. Nizk. Temp. **7**, 1305 (1981) [Sov. J. Low Temp. Phys. **7**, 634 (1981)]; B. Kuchta, T. Luty, and R. J. Meier, J. Phys. C **20**, 585 (1987).

[13] M. Minenko, M. Vetter, A. P. Brodyanski, and H. J. Jodl, Fiz. Nizk. Temp. **26**, 947 (2000) [Low Temp. Phys. **26**, 699 (2000)].

[14] P. M. Mathai and E. J. Allin, Can. J. Phys. **48**, 1518 (1970); **49**, 1973 (1971).

[15] K. D. Bier and H. J. Jodl, J. Chem. Phys. **81**, 1192 (1984).

[16] T. G. Blocker, M. A. Kinch, and F. G. West, Phys. Rev. Lett. **22**, 853 (1969); E. J. Wachtel and R. G. Wheeler, *ibid.* **24**, 233 (1970).

[17] A. de Bernabe, F. J. Bermejo, A. Criado, C. Prieto, F. Dunstetter, J. Rodriguez-Carvajal, G. Coddens, and R. Kahnn, Phys. Rev. B **55**, 11 060 (1997).

[18] E. J. Wachtel and R. G. Wheeler, J. Appl. Phys. **42**, 1581 (1971).

[19] A. P. J. Jansen and A. van der Avoird, J. Chem. Phys. **86**, 3583 (1987).

[20] R. D. Etters, A. A. Helmy, and K. Kobashi, Phys. Rev. B **28**, 2166 (1983).

[21] Yu. B. Gaididei, V. M. Loktev, A. F. Prikhot'ko, and L. I. Shanskii, Zh. Eksp. Teor. Fiz **68**, 1706 (1975) [Sov. Phys. JETP **41**, 855 (1975)].

[22] J. H. Van Vleck, Astrophys. J. **80**, 161 (1934).

[23] V. I. Dianov-Klokov, Opt. Spectrosc. **7**, 377 (1959); **13**, 109 (1962); **20**, 530 (1966).

[24] R. P. Blickensderfer and G. E. Ewing, J. Chem. Phys. **51**, 873 (1969).

[25] A. Landau, E. J. Allin, and H. L. Welsh, Spectrochim. Acta **18**, 1 (1962).

[26] One frequency value was given by A. F. Prikhot'ko, Mol. Cryst. Liq. Cryst. **57**, 189 (1980) for α-O_2. However, there is no concrete explanation, how this value was obtained from spectra.

[27] E. G. Petrov, V. M. Loktev, and Yu. B. Gaididei, Phys. Status Solidi **41**, 117 (1970).

[28] R. Bhandari and L. M. Falikov, J. Phys. C **6**, 479 (1973).

[29] T. Fujiwara, J. Phys. Soc. Jpn. **36**, 1530 (1974).
[30] P. Varasani and S. Sarangi, J. Quant. Spectrosc. Radiat. Transf. **15**, 473 (1975); B. Schurin and R. E. Ellis, J. Chem. Phys. **45**, 2528 (1966); C. L. Korb, R. H. Hunt, and E. K. Plyler, *ibid.* **48**, 4252 (1968).
[31] H. Kiefte and M. J. Clouter, J. Chem. Phys. **62**, 4780 (1975); A. F. Prikhotko, Yu. G. Pikus, and L. I. Shanskii, Opt. Spektrosk. **54**, 470 (1983) [Opt. Spectrosc. **54**, 277 (1983)].
[32] A. F. Prikhotko, V. S. Ostrovskii, Yu. G. Pikus, and L. I. Shanskii, Ukr. Phys. J. **25**, 1003 (1980).
[33] C. W. Cho, E. J. Allin, and H. J. Welsh, J. Chem. Phys. **25**, 371 (1956).
[34] Yu. B. Gaididei, V. M. Loktev, A. F. Prikhot'ko, and L. I. Shanskii, in *Cryocrystals*, edited by B. I. Verkin and A. F. Prikhot'ko (Naukova Dumka, Kiew, 1983), p. 231 (in Russian).
[35] G. C. Tabisz, E. J. Allin, and H. L. Welsh, Can. J. Phys. **47**, 2859 (1969).
[36] G. Zumofen and K. Dressler, J. Chem. Phys. **64**, 5198 (1976).
[37] S. Medvedev, A. P. Brodyanski, and H. J. Jodl (unpublished).
[38] H. Poulet and J. P. Mathieu, *Vibration Spectra and Symmetry of Crystals* (Gordon and Breach, New York, 1976).
[39] M. M. Thiery and V. Chandrasekharan, J. Chem. Phys. **67**, 3659 (1977).
[40] R. D. Beck, M. F. Hineman, and J. W. Nibler, J. Chem. Phys. **92**, 7068 (1990); R. Ouillon, C. Turc, J.-P. Lemaistre, and P. Ranson, *ibid.* **93**, 3005 (1990).
[41] D. A. Hatzenbuhler and L. Andrews, J. Chem. Phys. **56**, 3398 (1972).
[42] ''*PeakFit*'' *Peak Separation and Analysis Software* (AISN Software Inc., San Rafael, CA, 1995).
[43] Yu. B. Gaididei, V. M. Loktev, and A. F. Prikhot'ko, Fiz. Nizk. Temp. **3**, 1134 (1977) [Sov. J. Low Temp. Phys. **3**, 549 (1977)].
[44] *Tables of Isotopes*, 7th ed., edited by C. M. Lederer and V. S. Shirley (Wiley, New York, 1978).
[45] G. Herzberg, *Molecular Spectra and Molecular Structure I. Spectra of Diatomic Molecules* (Van Nostrand Reinhold, New York, 1950).
[46] C. Uyeda, K. Sugiyama, and M. Date, J. Phys. Soc. Jpn. **54**, 1107 (1985).
[47] P. W. Stephens and C. F. Majkrzak, Phys. Rev. B **33**, 1 (1986).
[48] P. E. S. Wormer and Ad van der Avoird, J. Chem. Phys. **81**, 1929 (1984).
[49] M. A. Buldakov, B. V. Korolev, I. I. Matrosov, and T. N. Popova, Opt. Spektrosk. **62**, 519 (1987) [Opt. Spectrosc. **62**, 309 (1987)].
[50] *Gas Encyclopedia*, English translation by Nissim Marshall (Elsevier, Amsterdam, 1976).
[51] A. P. Brodyanski and H. J. Jodl (unpublished).
[52] R. LeSar and R. D. Etters, Phys. Rev. B **37**, 5364 (1988).
[53] In their x-ray study, A. S. Baryl'nik, and A. I. Prokhvatilov, Fiz. Nizk. Temp. **20**, 912 (1994) [Low Temp. Phys. **20**, 716 (1994)] observed a surprisingly large (within 1 K) two-phase coexistence region by x-ray studies and did not detect any hysteresis.
[54] I. M. Vitebskii, V. L. Sobolev, A. A. Chabanov, and V. M. Loktev, Fiz. Nizk. Temp. **18**, 1044 (1992) [Sov. J. Low Temp. Phys. **18**, 733 (1992)]; **19**, 151 (1993) [**19**, 107 (1993)].
[55] (a) Yu. G. Litvinenko, V. V. Eremenko, and T. I. Garber, Zh. Eksp. Teor. Fiz., Pis'ma Red. **7**, 378 (1968) [JETP Lett. **7**, 298 (1968)]; (b) Phys. Status Solidi **30**, 49 (1968); (c) Ukr. Phys. J. **14**, 327 (1969).
[56] The value of 7940 cm^{-1} for the frequency of a principal maximum of the $^3\Sigma_g^-$-$^1\Delta_g$(0-0) absorption band in the α-O_2, given in Ref. 55(c) is contrary to present studies and data by others (Refs. 21 and 25).
[57] A. F. Prikhotko and L. I. Shanskii, Opt. Spectrosc. **33**, 490 (1972).